

## Three-dimensional modeling and inversion of x-ray pinhole detector arrays

K. Tritz, D. Stutman, L. Delgado-Aparicio, and M. Finkenthal

*Department of Physics and Astronomy, The Johns Hopkins University, 3400 North Charles Street, Baltimore, Maryland 21218*

(Received 7 May 2006; presented on 11 May 2006; accepted 16 June 2006; published online 26 September 2006)

X-ray pinhole detectors are a common and useful diagnostic for high temperature and fusion-grade plasmas. While the measurements from such diagnostics are line integrated, local emission can be recovered by inverting or modeling the data using varying assumptions including toroidal symmetry, flux surface isoemissivity, and one-dimensional (1D) chordal lines of sight. This last assumption is often valid when the structure sizes and gradient scale lengths of interest are much larger than the spatial resolution of the detector elements. However, x-ray measurements of, for example, the strong gradients in the *H*-mode pedestal may require a full three-dimensional (3D) treatment of the detector geometry when the emission of the plasma has a significant variation within the field of view, especially in a high-triangularity, low aspect ratio plasma. Modeling of a high spatial resolution tangential edge array for NSTX has shown that a proper 3D treatment can improve the effective spatial resolution of the detector by 10%–40% depending on the modeled signal-to-noise ratio and gradient scale length. Results from a general treatment of arbitrary detector geometry will provide a guideline for the amount of systematic error that can be expected by a 1D versus 3D field of view analysis. © 2006 American Institute of Physics. [DOI: [10.1063/1.2229188](https://doi.org/10.1063/1.2229188)]

### I. INTRODUCTION

The measurement of intensity using a multipixel detector or arrays of single detector elements is a common diagnostic tool in many areas of scientific research, plasma physics being no exception. Also common is the tendency to approximate the field of view (FOV) of each pixel or detector element as a thin “pencil beam,” thus ignoring the finite height and width of the beam. For many detector geometries, this simplification is quite valid as the systematic geometric errors introduced by such an approximation are on a scale much smaller than the scale of the features being measured. However, when the scale of the measured phenomena is on the order of the width of the FOV, then a complete three-dimensional (3D) treatment of the geometry of the detection elements will allow a more accurate reconstruction of the data. This work will investigate the variation between the one-dimensional (1D) and 3D modelings of detectors for plasma emission measurements, specifically for soft x-ray (SXR) pinhole detector arrays on the National Spherical Tokamak Experiment (NSTX).

### II. RESPONSE EQUATIONS FOR 1D AND 3D FOV CALCULATIONS

Intensity measured by a detector using the 1D pencil beam approximation is calculated by integrating the local plasma emission along a chordal line of sight

$$I = \int \varepsilon[R(l), Z(l), \varphi(l)] dl, \quad (1)$$

where the local emission is specified in cylindrical coordinates. An assumption of toroidal symmetry for the plasma emission removes the dependence on  $\varphi$ , and a detector geometry with a horizontal FOV removes the dependence on  $Z$ .

Conversion of the integral to cylindrical coordinates with the proper bounds then recovers the familiar Abel equation

$$I(R_{\text{tan}}) = 2 \int_{R_{\text{tan}}}^{R_a} \frac{\varepsilon(R) R dR}{\sqrt{R^2 - R_{\text{tan}}^2}}, \quad (2)$$

where  $R_{\text{tan}}$  is the tangency radius of the detector viewing chord and  $R_a$  is the outer radius of the plasma. As the emission and intensity profiles are often not described as analytic functions of  $R$ , the problem is usually discretized and translated to a cylindrical grid where the emission is assumed to be constant in each radial “zone.” The intensity of a detector element can then be described as the total sum of the product of each radial zone emission with a corresponding geometric “weighting factor” which is merely the detector chordal path length for that radial zone.

If the emission is not toroidally symmetric or the detector geometry FOV is not horizontal, then this simple Abel model cannot be applied. Also, if the scale of the emission variation is on the same order as the FOV width, then the simple model will not accurately reconstruct the measured detector intensity. In either case, a full 3D treatment of the emission and detector response can provide an accurate model for intensity calculations. The fundamental process of generating the detector intensity is similar to the 1D case. The intensity is calculated as the volume integral of the product of the plasma emission and a 3D geometric weighting factor describing the detector response. Again, the product is discretized and translated to a cylindrical grid where the intensity can be represented by the sum of the emission and detector response for a given grid volume element.

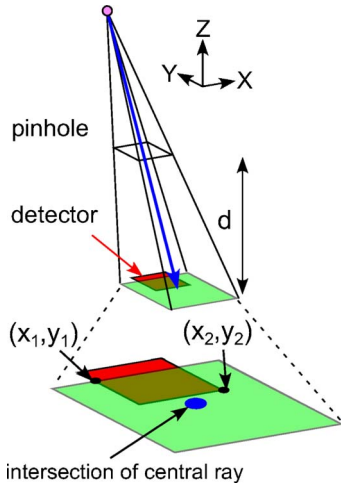


FIG. 1. Geometry of detector point response function showing overlap of projection with detector area.

$$I \approx \sum_{i,j,k} \varepsilon_{i,j,k} g_{i,j,k}. \quad (3)$$

Here,  $i$ ,  $j$ , and  $k$  represent the indices for the radial, vertical, and toroidal grid coordinates, respectively, while  $\varepsilon$  is the plasma emission, and  $g$  is the geometric detector response for the corresponding grid volume element.

The geometric detector response,  $g_{i,j,k}$ , is calculated by performing the 3D integral of the detector point response function over the cylindrical grid element volume specified by the indices  $i$ ,  $j$ , and  $k$ .

$$g_{i,j,k} = \int_{R_i-dR/2}^{R_i+dR/2} R dR \int_{Z_j-dZ/2}^{Z_j+dZ/2} dZ \int_{\varphi_k-d\varphi/2}^{\varphi_k+d\varphi/2} p(R, Z, \varphi) d\varphi. \quad (4)$$

The detector point response function,  $p$ , is merely the solid angle of a point in the specified volume element subtended by the area of the detector element. This point response depends on the square of the distance between the point and the detector, and also the angle formed relative to the optical axis of the detector. A precise calculation of the point response involves integration of the distance and angular dependence over the region of overlap, as shown in Fig. 1. It is convenient to transform the coordinate system to a Cartesian grid with the origin at the center of the pinhole and the  $z$  axis aligned with the optical axis of the detector. The point response function can then be described as

$$p = \frac{z^4}{4\pi(z+d)^2} \int_{y_1}^{y_2} \frac{dy}{\sqrt{y^2+z^2}} \int_{x_1}^{x_2} \frac{dx}{\sqrt{x^2+z^2(x^2+y^2+z^2)}}, \quad (5)$$

where  $p$  is the point response function,  $d$  is the distance between the detector and the pinhole,  $x$ ,  $y$ , and  $z$  are the Cartesian distances from the pinhole to the specified point,  $(R, Z, \varphi)$  inside the cylindrical volume element, and  $(x_1, y_1)$  and  $(x_2, y_2)$  represent the coordinates of the region of overlap between the detector element and the projection of the point through the pinhole. For typical detector and pinhole geometries, the variation of the functions inside the integrals is

small for points located away from the pinhole ( $z > d$ ). Thus, the point response function can be approximated by the product of the value calculated from the central chord and the total area of the overlap region.

$$p \approx \frac{1}{4\pi} \frac{(x_2-x_1)(y_2-y_1)z^4}{\sqrt{x^2+z^2}\sqrt{y^2+z^2}(x^2+y^2+z^2)(z+d)^2}. \quad (6)$$

This approximation is good to  $\ll 1\%$  for typical detector geometries, for example, the variation is within  $1 \times 10^{-4}$  for a point with  $z=0.5$  m and a detector width of 1 cm.

With this approximation for the detector point response, the detector response element,  $g_{i,j,k}$ , can then be calculated by transforming  $p$  back to cylindrical coordinates and integrating over the volume element. The analytic integration of  $p$  for an arbitrary detector geometry is a fairly intractable problem, so 3D Gaussian quadrature numerical integration is used with the ability to scale the number of integration points,  $N$ , along each dimension to provide control over calculation accuracy and computational speed.<sup>1</sup> The calculation time scales with the total number of integrations  $\sim N^3$ , but the error in the results is  $< 1\%$  for  $N > 6$  and reaches a minimum near  $N=12$ . At  $N > 32$ , the error begins to increase again as the limits in machine computational precision are reached.

Numerical evaluation of the volume integral for every element of the cylindrical grid is both inefficient and computationally impractical as the total number of volume elements for a typical grid is  $O(10^6)$ . Therefore, a simple recursive algorithm is used to generate a list of only those elements, and their corresponding geometric response, which contribute to the overall detector response. The algorithm searches the cylindrical grid by integrating the response along one particular coordinate direction until it finds an element with a zero response. The algorithm path then changes coordinate direction until it hits another boundary. This process reduces the number of integral evaluations to  $O(10^3)$ . Finally, while the IDL language is used for the main setup and display of the detector calculations, the numerical integration operated too inefficiently even using optimized IDL code. Writing the 3D detector response code in C and linking the code into IDL afforded a speed up by  $\times 40$ . The calculation time of the response of a detector element with  $N=12$ ,  $65 \times 65 \times 360$  grid, is  $O(1$  s).

### III. MODELING OF HIGH SPATIAL RESOLUTION EDGE SXR ARRAY

One of the primary motivations for this work was the consideration of and proposal for a new, high spatial resolution SXR array that has a tangential view of the NSTX plasma edge, with  $R_{\text{tan}} \sim 135-155$  cm [Fig. 2(a)]. This array would use radial spatial resolution  $\leq 1$  cm to focus on the sharp edge gradients typical of  $H$ -mode plasmas in NSTX and be used to study the boundary stability and associated phenomena (e.g., edge localized modes (ELMs)). This resolution criterion required a horizontal width of the detector and pinhole element of  $\sim 1$  mm. However, to achieve a rea-

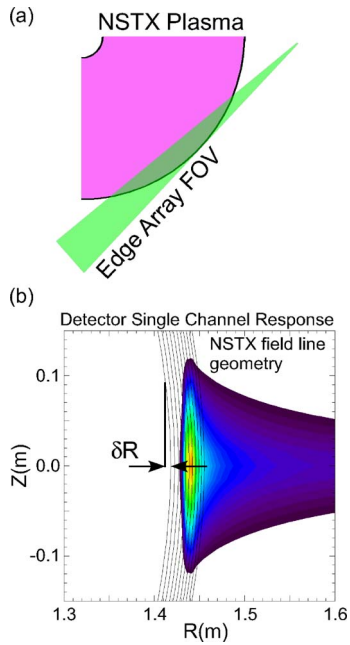


FIG. 2. (a) Field of view sketch of proposed SXR edge array on NSTX. (b) Edge array single channel detector response overlaid on plot showing radial displacement due to flux surface curvature on NSTX.

sonable optical throughput, the system was designed with a pinhole and vertical height of 16 mm resulting in a total étendue of  $2.6 \times 10^{-8} \text{ m}^2/\text{sr}$ .

The specified pinhole and detector geometry results in a spot size in the plasma with a corresponding vertical resolution of  $\sim 16 \text{ cm}$  [Fig 2(b)]. At this length scale, the curvature of the magnetic flux surfaces can cause a radial deviation across the height of the sampling volume according to the following geometric relationship:<sup>2</sup>

$$\delta R \approx \frac{1 + \delta Z^2}{\kappa^2 a}, \quad (7)$$

where  $\delta R$  is the radial deviation,  $\delta$  and  $\kappa$  are the triangularity and elongation, respectively, for the flux surface of interest,  $a$

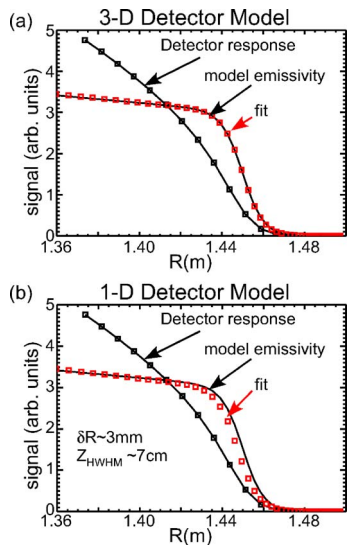


FIG. 3. (a) 3D response model and (b) 1D response model of detector response and fitting to tanh emission profile.

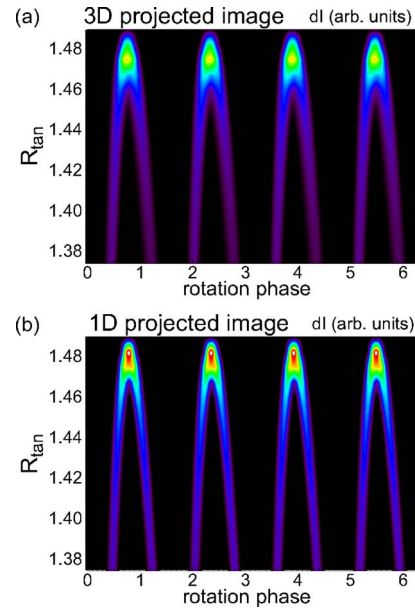


FIG. 4. (a) 3D model projection and (b) 1D model projection of helical perturbation emission viewed by edge array.

is the minor radius of the flux surface, and  $Z$  is the “half-width half maximum” (HWHM) of the vertical resolution. For a detector with  $R_{\text{tan}} \sim 143 \text{ cm}$  ( $Z_{\text{HWHM}} \sim 7 \text{ cm}$ ) and typical NSTX plasma parameters ( $a=45 \text{ cm}$ ,  $\kappa=2.0$ , and  $\delta=0.3$ ), the radial deviation caused by the flux surface curvature,  $\delta R$ , is  $\sim 3 \text{ mm}$ .

The effects of this radial deviation can be examined by comparing the 1D and 3D detector intensity and corresponding emissivity reconstruction of a model emission profile containing a sharp gradient at the plasma edge. The emission model used is a hyperbolic tangent function which can be adjusted with parameters controlling the pedestal radial location,  $R_{\text{ped}}$ , width,  $w_{\text{ped}}$ , height,  $A_{\text{ped}}$ , and slope of the emission,  $S(R)$ , from the top of the pedestal to the core.

$$\varepsilon(R) = A_{\text{ped}} \left\{ \frac{1 + \tanh[(R_{\text{ped}} - R)/w_{\text{ped}}]}{2} + S(R) \right\}. \quad (8)$$

This function is used both to create the emission profile and also to fit the forward modeling reconstruction. The reconstructed profile is calculated by generating the emission profile, calculating the detector response, adding a combination of photon and overall system noise, and using these synthetic data with a forward modeling nonlinear fitting routine to fit the four function parameters. The fitted data using the full 3D model response could accurately reconstruct the model emission profile even with 5%–10% photon noise and 1%–3% overall system noise. However, the fitted profile using the 1D response matrix systematically fits to a smaller pedestal location,  $\delta R_{\text{ped}} \sim 3 \text{ mm}$ , which is consistent with the predicted radial flux surface deviation (Fig. 3). While 3 mm may be negligible for many SXR imaging systems, it constitutes  $\sim 30\%$  of the desired spatial resolution of the edge array. As such, a full 3D treatment of the high spatial resolution tangential edge array is necessary for accurate gradient imaging and reconstruction.

Another interesting edge phenomenon observed on NSTX is the existence of small ELMs which have a helical structure that is fairly localized both toroidally and poloidally.<sup>3</sup> These ELMs have been imaged with the current set of poloidal SXR arrays along with many other diagnostics, but the analysis of these phenomena could benefit from a measurement with higher radial spatial resolution that can probe the plasma pedestal. To see if the edge SXR array would provide a useful image, the previous pedestal model with an *ad hoc* helical filament perturbation was used to examine the differences in imaging between the 3D and 1D models. As can be seen in Fig. 4, the 1D model image provides a sharper projection which is shifted radially outward, again by  $\sim \delta R$ . Therefore, use of the 1D model to interpret the measured image, which should more closely resemble the more accurate 3D model, would result in the reconstruction of a filament at a shifted radial location with a larger, more diffuse, emission profile.

An edge SXR array with high radial resolution offers the possibility to examine in detail a region of the NSTX plasma which is presently under-resolved by the current diagnostic set. This diagnostic, coupled with an accurate, fully 3D model of the detector geometric response, will provide  $\sim 1$  cm radial resolution while maintaining enough optical throughput for a good signal-to-noise ratio.

## ACKNOWLEDGMENTS

This work has been supported by US DOE Grant No. DE-FG02-99ER5452. Thanks and appreciation to the NSTX team for their support.

<sup>1</sup>W. H. Press, *Numerical Recipes in C: The Art of Scientific Computing* (Cambridge University Press, New York, 1992), p. 147.

<sup>2</sup>F. Albajar Viñas, PhD thesis, Department of Nuclear Engineering, Polytechnic Institute of Catalunya, 2001.

<sup>3</sup>R. Maingi *et al.*, *Nucl. Fusion* **45**, 264 (2005).